Evolution of magnetic properties in the vicinity of the Verwey transition in Fe_3O_4 thin films

X. H. Liu,[1,2,*] W. Liu,[2] and Z. D. Zhang[2]

[1]*Max Planck Institute for Chemical Physics of Solids, Nöthnitzerstraße 40, 01187 Dresden, Germany*

[2]*Shenyang National Laboratory for Materials Science, Institute of Metal Research, Chinese Academy of Sciences, Shenyang 110016, China*

(Received 7 May 2017; revised manuscript received 20 July 2017; published 5 September 2017)

We have systematically studied the evolution of magnetic properties, especially the coercivity and the remanence ratio in the vicinity of the Verwey transition temperature (T_V), of high-quality epitaxial Fe_3O_4 thin films grown on MgO (001), $MgAl_2O_4$ (MAO) (001), and $SrTiO_3$ (STO) (001) substrates. We observed rapid change of magnetization, coercivity, and remanence ratio at T_V, which are consistent with the behaviors of resistivity versus temperature [$\rho(T)$] curves for the different thin films. In particular, we found quite different magnetic behaviors for the thin films on MgO from those on MAO and STO, in which the domain size and the strain state play very important roles. The coercivity is mainly determined by the domain size but the demagnetization process is mainly dependent on the strain state. Furthermore, we observed a reversal of remanence ratio at T_V with thickness for the thin films grown on MgO: from a rapid enhancement for 40-nm- to a sharp drop for 200-nm-thick film, and the critical thickness is about 80 nm. Finally, we found an obvious hysteretic loop of coercivity (or remanence ratio) with temperature around T_V, corresponding to the hysteretic loop of the $\rho(T)$ curve, in Fe_3O_4 thin film grown on MgO.

DOI: 10.1103/PhysRevB.96.094405

I. INTRODUCTION

Magnetite (Fe_3O_4) is one of the most important transition-metal oxides and is being actively investigated due to its rather unique and interesting set of electrical and magnetic properties, such as the high Curie temperature (858 K), relatively high saturation magnetization, small coercivity field [1,2], theoretically predicted half-metallic behavior [3–6], and the famous first-order metal-insulator transition at 124 K (known as the Verwey transition) [7]. These make Fe_3O_4 a potential candidate for spin electronic devices, such as spin valves or spin tunnel junctions [8–14]. However, it has been very difficult to realize these unique properties in thin films for various device applications, owing to the uncontrollable formation of growth defects, such as antiphase boundaries (APBs) [15,16]. It has been reported that the APBs generally exist in epitaxial Fe_3O_4 thin films grown on MgO, sapphire, $MgAl_2O_4$, or $SrTiO_3$ substrates due to the lower symmetry and twice the lattice constant of Fe_3O_4 ($Fd\bar{3}m$) with respect to MgO ($Fm\bar{3}m$) and the large lattice mismatch for the other substrates [14–50]. Numerous studies have shown that because of the presence of APBs in Fe_3O_4 thin films, their transport and magnetic properties strongly deviate from the single-crystal bulk, such as the low Verwey transition temperature (T_V) and very broadened transition, and an increased resistivity with decreasing film thickness [14,18–27,29–35,37,38], negative unsaturated magnetoresistance [14,18–23,25–27,33], superparamagnetic behavior in ultrathin films [41,42], and nonsaturation magnetization at very high fields [15–17,46,47]. Recently, Liu *et al.* [51] obtained exceptionally high quality Fe_3O_4 thin films grown on tailored spinel $Co_{2-x-y}Mn_xFe_yTiO_4$ substrates with relatively small lattice mismatch, which not only exhibit the Verwey transition as sharply as the single-crystal bulk but also present quite high T_V up to 136.5 K. This work gives an example of the better Verwey transition in Fe_3O_4 thin films than in the single-crystal bulk. It is clear that the Fe_3O_4 thin films without APBs show intrinsic transport properties, which are quite different from those of films grown on general substrates [14,18–27,29–35,37,38]. However, the magnetic $Co_{2-x-y}Mn_xFe_yTiO_4$ substrates greatly restrict the study in magnetic properties of these Fe_3O_4 thin films.

The magnetic properties of bulk Fe_3O_4 have been widely studied in the past several decades [52–60]. With lowering temperature across the Verwey transition, the transformation from cubic to monoclinic structure leads to a sharp jump for some magnetic parameters at T_V, such as the rapid drop of magnetization and the sharp enhancement of coercivity. On the other hand, although a tremendous amount of work has been devoted to investigating the magnetic properties of Fe_3O_4 thin films [14–18,20,33,34,39–42,44–50], the systematic study of magnetic properties of the thin films in the vicinity of the Verwey transition has been seldom reported [44,45]. Bollero *et al.* [44] investigated the influence of thickness on microstructural and magnetic properties in Fe_3O_4 thin films. They gave out the variation of coercivity and remanence across the T_V, and the APBs are considered to significantly affect the magnetization behaviors of Fe_3O_4 thin films. In previous work, however, the Verwey transition in Fe_3O_4 thin films was very broad and the T_V was quite low; the quality of these thin films should not be high enough (the presence of chemical off stoichiometry or many APBs), which would greatly influence the magnetic properties. In our previous work, we have grown quite high quality epitaxial Fe_3O_4 thin films; the Verwey transition is very sharp and the T_V reaches to 122 K for 200-nm-thick Fe_3O_4 film on MgO (001) [37], which is close to that of the single-crystal bulk and much higher than in previous work [15–17,41–50]. Therefore, to more comprehensively understand the magnetic behaviors in Fe_3O_4 thin films, it is very necessary to reinvestigate the magnetic properties in high-quality Fe_3O_4 thin films.

In this work, we systematically investigate the evolution of magnetic properties with temperature of high-quality epitaxial Fe_3O_4 thin films grown on MgO (001), $MgAl_2O_4$ (MAO)

*xhliu@alum.imr.ac.cn

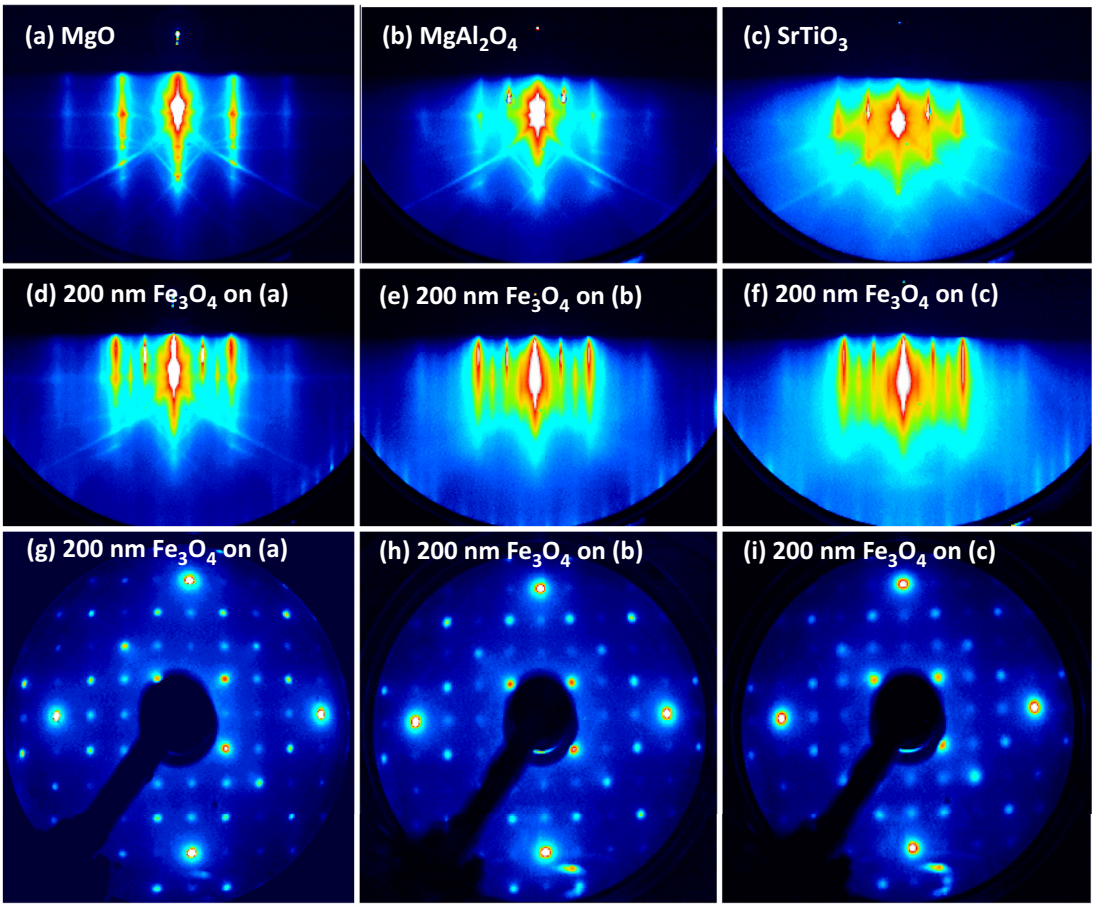

FIG. 1. RHEED electron diffraction patterns of the following: the clean MgO (001) (a), $MgAl_2O_4$ (001) (b), and $SrTiO_3$ (001) (c); RHEED and LEED electron diffraction patterns of 200-nm-thick Fe_3O_4 films grown on MgO (001) (d) and (g), MAO (001) (e) and (h), and STO (001) (f) and (i).

(001), and $SrTiO_3$ (STO) (001) substrates. Rapid changes of magnetization, coercivity, and remanence ratio were observed at T_V, which are in agreement with the behaviors of resistivity versus temperature [$\rho(T)$] curves for different thin films. Especially, the thin film grown on MgO was found to exhibit quite different magnetic behavior from that on MAO and STO, in which the domain size and the strain state take the dominate role. The coercivity is mainly determined by the domain size but the demagnetization process is mainly related to the strain state. The small domain size and high strain state lead to large coercivity and incoherent reversal of magnetization, respectively. Furthermore, a very interesting reversal of remanence ratio with thickness, from a rapid increase for 40-nm- to a sharp drop for 200-nm-thick film, at T_V was noticed for the thin films grown on MgO, and the critical thickness is about 80 nm, which might be greatly related to interface effect of the thin films. At last, a clear hysteretic loop of coercivity (or remanence ratio) with temperature around the T_V, corresponding to the loop of the $\rho(T)$ curve, was observed in Fe_3O_4 thin film grown on MgO.

II. EXPERIMENTAL

Fe_3O_4 thin films were grown by molecular beam epitaxy (MBE) in an ultrahigh vacuum (UHV) chamber with a base pressure in the 1×10^{-10} mbar range. High-purity Fe metal was evaporated from a LUXEL Radak effusion cell at temperatures of about 1250 °C in a pure oxygen atmosphere onto single-crystalline MgO (001), $MgAl_2O_4$ (001) (MAO), and $SrTiO_3$ (001) (STO) substrates. These substrates were annealed for two hours at 600 °C in an oxygen pressure of 3×10^{-7} mbar to obtain a clean and well-ordered surface structure before the Fe_3O_4 deposition. Standard samples were grown using an iron flux of 1 Å/min, an oxygen background pressure of 1×10^{-6} mbar, and a growth temperature of 250 °C [37]. *In situ* and real-time monitoring of the epitaxial growth was performed by reflection high-energy electron diffraction (RHEED) measurements. Oscillations in the RHEED specular beam intensity, where each oscillation corresponds to the formation of one new atomic monolayer (ML), allows for precise control of the film thickness. The crystalline structure was also verified *in situ* after the growth by low-energy electron diffraction (LEED). The RHEED patterns were taken at 20 keV electron energy, with the beam aligned parallel to the [100] direction of the substrate and the LEED patterns were recorded at an electron energy of 88 eV. Furthermore, all samples were analyzed *in situ* by x-ray photoelectron spectroscopy (XPS). The XPS data were collected using 1486.6 eV photons (monochromatized Al K_α light) in normal emission geometry and at room temperature using a Scienta R3000 electron energy

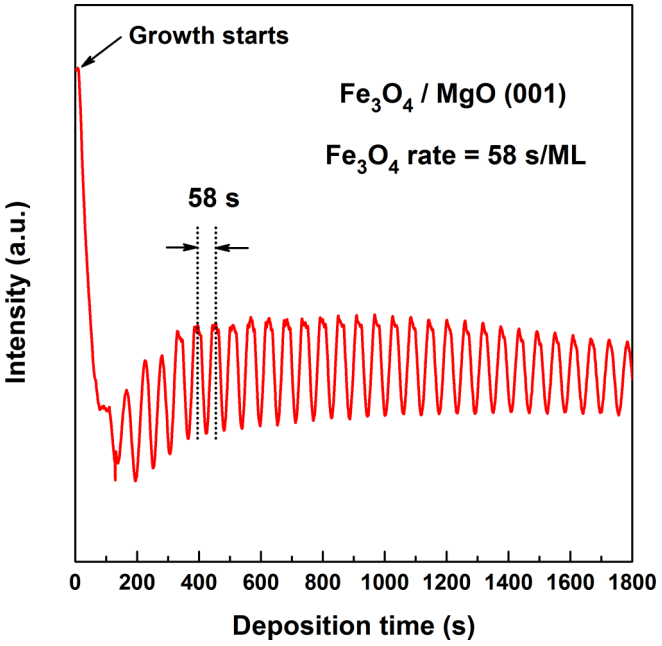

FIG. 2. RHEED intensity oscillations of the specularly reflected electron beam recorded during deposition of Fe_3O_4 thin film on MgO (001) substrate.

analyzer. The overall energy resolution was set to about 0.3 eV. Measurements for temperature dependence of transport and magnetic properties of Fe_3O_4 thin films were performed with the standard four-probe technique using a physical property measurement system (PPMS) and a superconducting quantum interference device (SQUID), respectively. X-ray diffraction (XRD) was employed for further *ex situ* investigation of the structural quality and the microstructure of the samples. The XRD measurements were performed with a high-resolution PANalytical X'Pert MRD diffractometer using monochromatic Cu $K_{\alpha 1}$ radiation ($\lambda = 1.54056$ Å).

III. MICROSTRUCTURAL CHARACTERIZATION

Figure 1 shows the RHEED patterns of clean substrates MgO (001) [Fig. 1(a)], MAO (001) [Fig. 1(b)], and STO (001) [Fig. 1(c)], and RHEED and LEED patterns of 200-nm-thick Fe_3O_4 thin films grown on MgO [Figs. 1(d) and 1(g)], MAO [Figs. 1(e) and 1(h)], and STO [Figs. 1(f) and 1(i)], respectively. The sharp RHEED streaks and the presence of Kikuchi lines, as well as the intense and sharp LEED spots [Figs. 1(d) and 1(g)] indicate a flat and well ordered (001) crystalline surface structure of the Fe_3O_4 thin film on MgO. Because the growth is fully coherent, with the in-plane dimensions of the spinel unit cell of Fe_3O_4 being twice those of the rocksalt unit cell of MgO, one expects a new set of diffraction rods (spots) occurring with half spacing of the substrate. The RHEED and LEED patterns indeed show the occurrence of the half-order diffraction rods (spots) in the zeroth Laue zone. The signature of the $(\sqrt{2} \times \sqrt{2})R45^\circ$ surface reconstruction, which is also characteristic for single-crystal magnetite, corresponding to a new set of diffraction rods and spots, is clearly observed in Figs. 1(d) and 1(g), respectively. At the same time, the typical RHEED and LEED images with the presence of

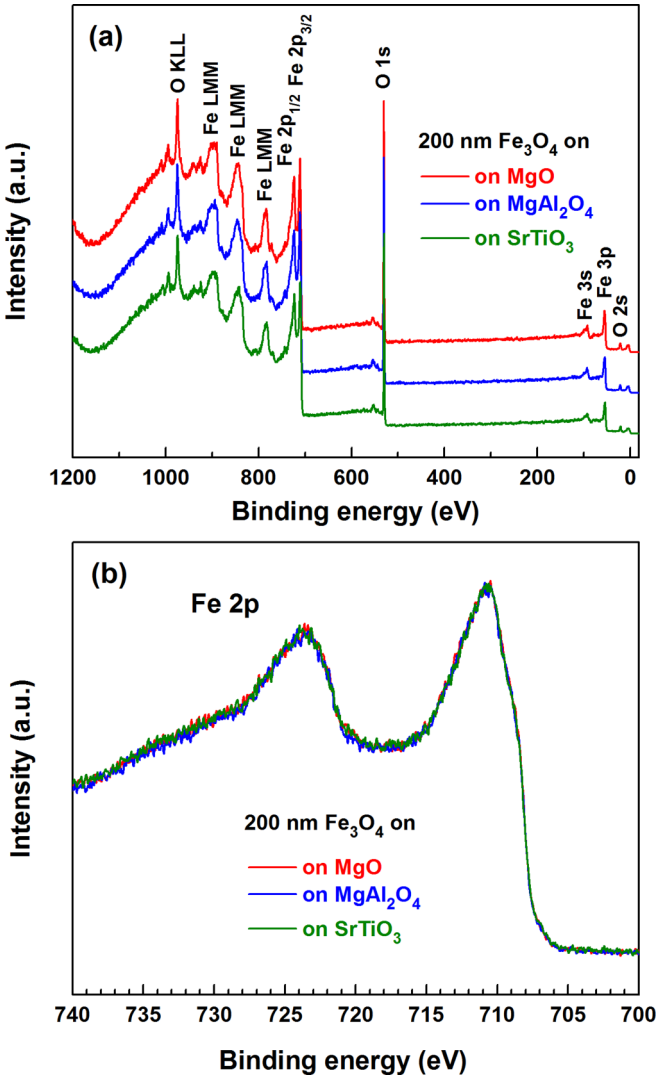

FIG. 3. XPS wide-scan spectra with binding energy from 1200 eV to −18 eV (a); Fe $2p$ core-level spectra (b) of 200-nm-thick Fe_3O_4 thin films grown on MgO (001), $MgAl_2O_4$ (001), and $SrTiO_3$ (001) substrates.

$(\sqrt{2} \times \sqrt{2})R45^\circ$ surface reconstruction are obviously seen for the films on MAO [Figs. 1(e) and 1(h)] and on STO [Figs. 1(f) and 1(i)], demonstrating also the high quality of these two Fe_3O_4 thin films. Moreover, we found that for the film grown on STO, the RHEED and LEED patterns become slightly weak and blurred, indicating a slightly increasing disorder in this film due to the large lattice mismatch (−7.5%). We have recorded the time development of the crystalline structure during the films growth. In Fig. 2 we can clearly observe pronounced intensity oscillations, which are indicative of a two-dimensional layer-by-layer growth; the time period of the oscillation is 58 s, which corresponds to the time needed to grow 1 ML of Fe_3O_4 and allows for a precise thickness determination.

In order to clarify the chemical state of the iron oxide, the wide scan with binding energy from 1200 to −18 eV and Fe $2p$ core level XPS spectra were *in situ* recorded for 200-nm-thick Fe_3O_4 thin films grown on MgO (001), MAO (001), and

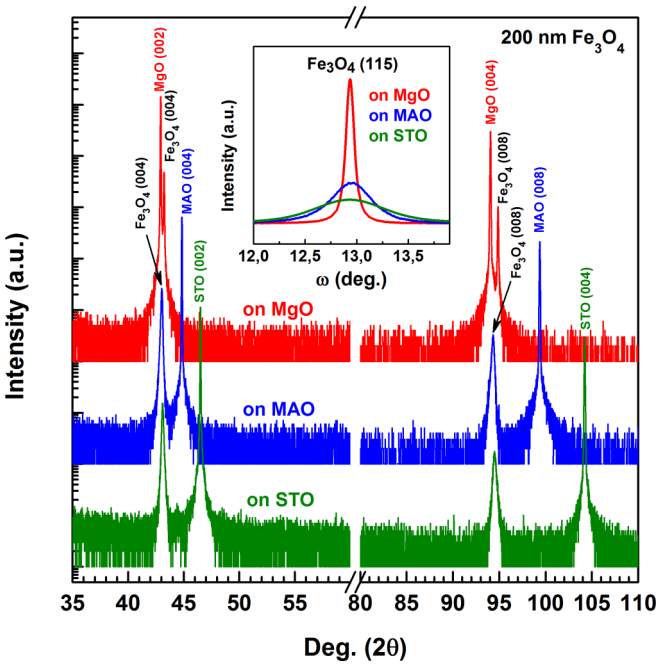

FIG. 4. X-ray diffraction patterns for 200-nm-thick Fe_3O_4 films grown on MgO (001) (red), $MgAl_2O_4$ (001) (blue), and $SrTiO_3$ (001) (olive), respectively. Inset: High-resolution rocking curves of the Fe_3O_4 (115) peak of these three films.

STO (001), as shown in Figs. 3(a) and 3(b), respectively. The XPS spectra in Figs. 3(a) and 3(b) demonstrate a quite clean surface and represent the typical signatures of Fe_3O_4 thin films [37,51,61,62]. The identical XPS spectra also indicates no influence of substrates on the chemical composition of the thin films. XRD experiments have been *ex situ* performed on 200-nm-thick Fe_3O_4 thin films grown on MgO, MAO, and STO, respectively, as shown in Fig. 4. It is found that the XRD patterns do not display any phase other than substrates and Fe_3O_4. For the samples grown on MgO (red color) and on STO (olive color), the (002)/(004) and (004)/(008) reflections correspond to MgO (or STO)/Fe_3O_4 because of the lattice constant of Fe_3O_4 as twice as that of MgO (or STO), and the (004) and (008) reflections for both MAO and Fe_3O_4 are presented for the blue color pattern. Moreover, with respect to the samples on MAO and STO, the Fe_3O_4 peaks of the sample on MgO obviously shift to a high degree due to the fully tensile strained state with reduction of lattice constant **c**. The fully relaxed state for samples on MAO and STO because of large lattice mismatch results in the same lattice constant, corresponding to the same degree θ, as that of the bulk; the strain state of the samples will be shown later. XRD rocking-curve measurements of the in-plane reflection (115) of the Fe_3O_4 thin films on MgO, MAO, and STO are displayed as an inset of Fig. 4. A sharp peak with quite small full width at half maximum (FWHM) can be seen for Fe_3O_4 thin film on MgO, while the samples grown on MAO and STO exhibit very broad peaks. By using the simple Scherrer formula [63], we calculated an average domain size of 98 nm, 20 nm, and 11 nm for 200-nm-thick Fe_3O_4 thin films grown on MgO, MAO, and STO, respectively, which is similar to our previous work [37].

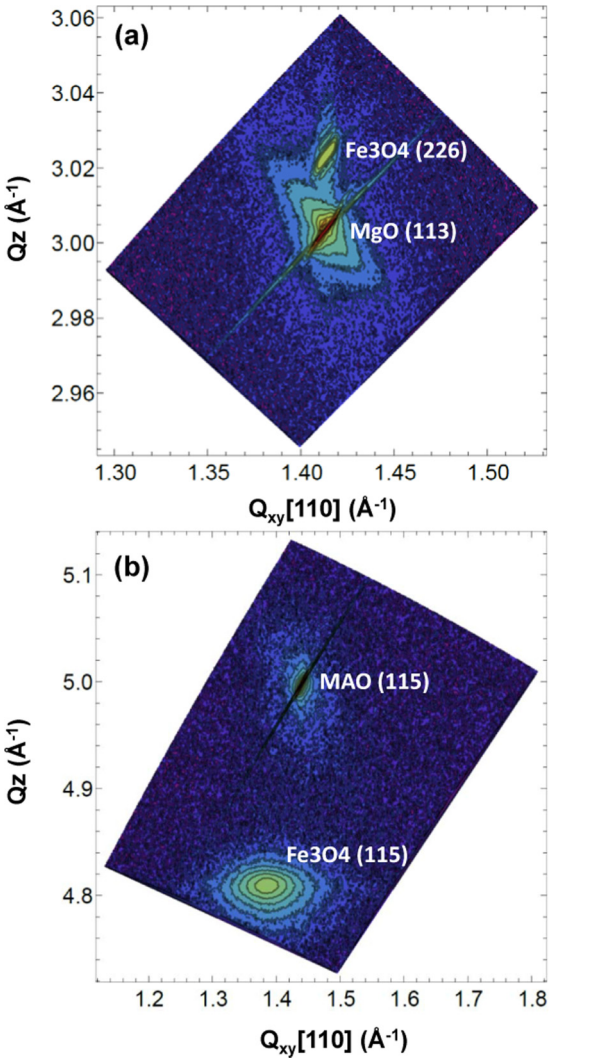

FIG. 5. Reciprocal space mapping in the vicinity of the asymmetrical MgO (113) and Fe_3O_4 (226) (a), and (115) reflection (b) of 200-nm-thick Fe_3O_4 films grown on MgO (001) and $MgAl_2O_4$ (001), respectively.

Furthermore, the strain state of the Fe_3O_4 thin films was also studied by XRD measurements. Figure 5 presents the reciprocal space mapping of the (226) and (115) reflections of 200-nm-thick Fe_3O_4 films grown on MgO (001) (a) and MAO (001) (b), respectively. Any lattice relaxation will result in a deviation of the (226) or (115) line; i.e., the satellite peaks will not line up with the substrate peak located at (226) and (115). Here, a relaxation rate can be defined as $R = (\mathbf{a}_{\text{film}} - \mathbf{a}_{\text{substrate}})/(\mathbf{a}_{\text{bulk}} - \mathbf{a}_{\text{substrate}})$, where $\mathbf{a}_{\text{film}}$ and $\mathbf{a}_{\text{substrate}}$ are the in-plane lattice parameters of the Fe_3O_4 thin film and substrate, respectively, and $\mathbf{a}_{\text{bulk}}$ is the lattice constant for bulk Fe_3O_4 (8.397 Å). According to this definition, $R = 0\%$ and 100% will correspond respectively to a fully strained and fully relaxed state of the thin film. In Fig. 5, fully strained and fully relaxed states can be obtained for 200-nm-thick Fe_3O_4 thin films grown on MgO [Fig. 5(a)] and MAO [Fig. 5(b)], respectively. Therefore, the critical thickness is bigger than 200 nm for Fe_3O_4 thin film grown on MgO, which is much larger than that calculated from the Fischer, Kuhne, and Richter

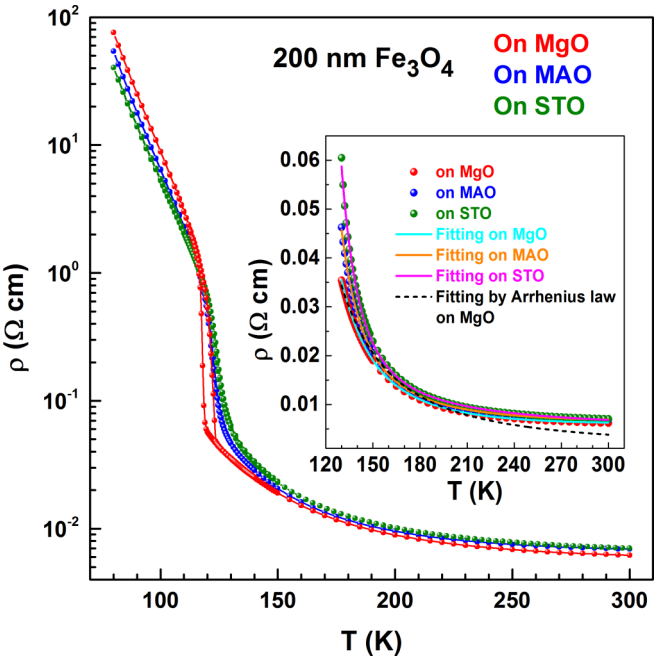

FIG. 6. Resistivity as a function of temperature for 200-nm-thick Fe_3O_4 films grown on MgO (001), $MgAl_2O_4$ (001), and $SrTiO_3$ (001), respectively. Inset: Temperature dependence of resistivity (from 130 to 300 K) and the fitting curves with nonadiabatic polaron model for the three films, as well as the fitting curve by Arrhenius law for the film on MgO (black dashed line).

model [64], but similar to that reported by Arora *et al.* [28]. The 200-nm-thick Fe_3O_4 thin film grown on MAO is fully relaxed due to the much larger lattice mismatch (−3.7%) [32,64]. However, in Bollero *et al.*'s work [44], the 320-nm-thick Fe_3O_4 film grown on MAO (001) still shows an 80% relaxation rate.

IV. TRANSPORT CHARACTERIZATION

Having investigated the microstructural characterization of the 200-nm-thick Fe_3O_4 thin films grown on different substrates, we then measured the transport properties of these samples. The resistivity as a function of temperature $\rho(T)$ for the 200-nm-thick Fe_3O_4 films grown on MgO (001), MAO (001), and STO (001) are presented in Fig. 6. Here the Verwey transition temperatures T_{V+} and T_{V-} are defined as the temperature of the maximum slope of the $\log[\rho(T)]$ curve for the warming up and cooling down temperature branches, respectively. It is observed that the film grown on MgO displays very sharp transition with T_{V+} of 122 K, close to that of the single-crystal bulk, whereas the transition becomes very broad with T_{V+} of around 124.5 K for the film grown on MAO or STO. From the XRD results we have obtained an average domain size of about 98 nm, 20 nm, and 11 nm for 200-nm-thick Fe_3O_4 films grown on MgO, MAO, and STO, respectively (see inset of Fig. 4). The observation of a broad transition implies more inhomogeneity for the latter two samples; i.e., they consist of a wide distribution of crystallites each having its own transition temperature [37]. The broadest Verwey transition induced from the smallest average domain size is seen for the film on STO, and a big hysteresis of about 4 K for the film on MgO would be attributed to the large density of

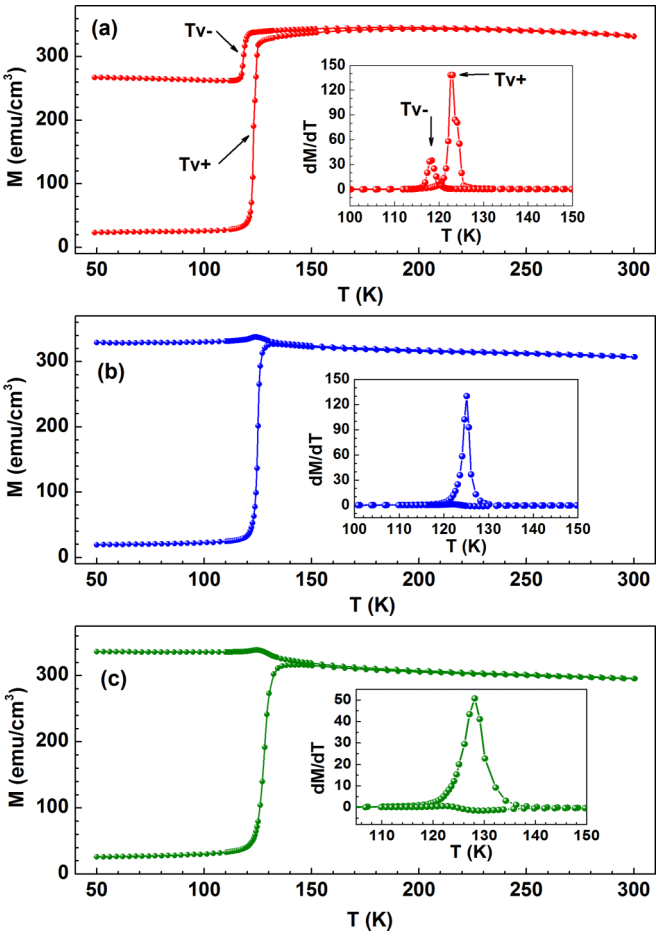

FIG. 7. ZFC-FC temperature-dependent magnetization curve of 200-nm-thick Fe_3O_4 films grown on MgO (001) (a), $MgAl_2O_4$ (001) (b), and $SrTiO_3$ (001) (c), in an applied field of 200 Oe. Insets: dM/dT as a function of temperature in the vicinity of Verwey transition temperature.

APBs [37]. To better understand the transport properties of the Fe_3O_4 thin films, we fitted the $\rho(T)$ curves above the Verwey transition (from 130 to 300 K) with an Arrhenius law: $\rho(T) = \rho_\infty \exp(E_a/kT)$ [21,30] and nonadiabatic polaron model: $\rho(T) = \rho_0 T^{3/2} \exp(E_a/kT - C/T^3 + D/T^5)$ [65]; here, E_a is an activation energy, and C and D are constant parameters. It is found that the fitting results are much better by using the latter model (see the inset of Fig. 6), and the activation energy is about 32 meV (about 43 meV by the Arrhenius law) for 200-nm-thick Fe_3O_4 film grown on MgO, which is much lower than 56 meV in Ref. [21] and 46 meV in Ref. [30]. At the same time, the Fe_3O_4 film grown on MAO or STO has a higher activation energy of 46 meV or 71 meV due to its much smaller average domain size. Therefore, the smaller the average domain size, the larger the activation energy, and the more difficult the hopping of the electrons in Fe_3O_4 thin films above T_V.

V. MAGNETIC CHARACTERIZATION

As shown in the above sections, the microstructural characterization and the transport property measurements indicate the high quality of our Fe_3O_4 thin films. We began the

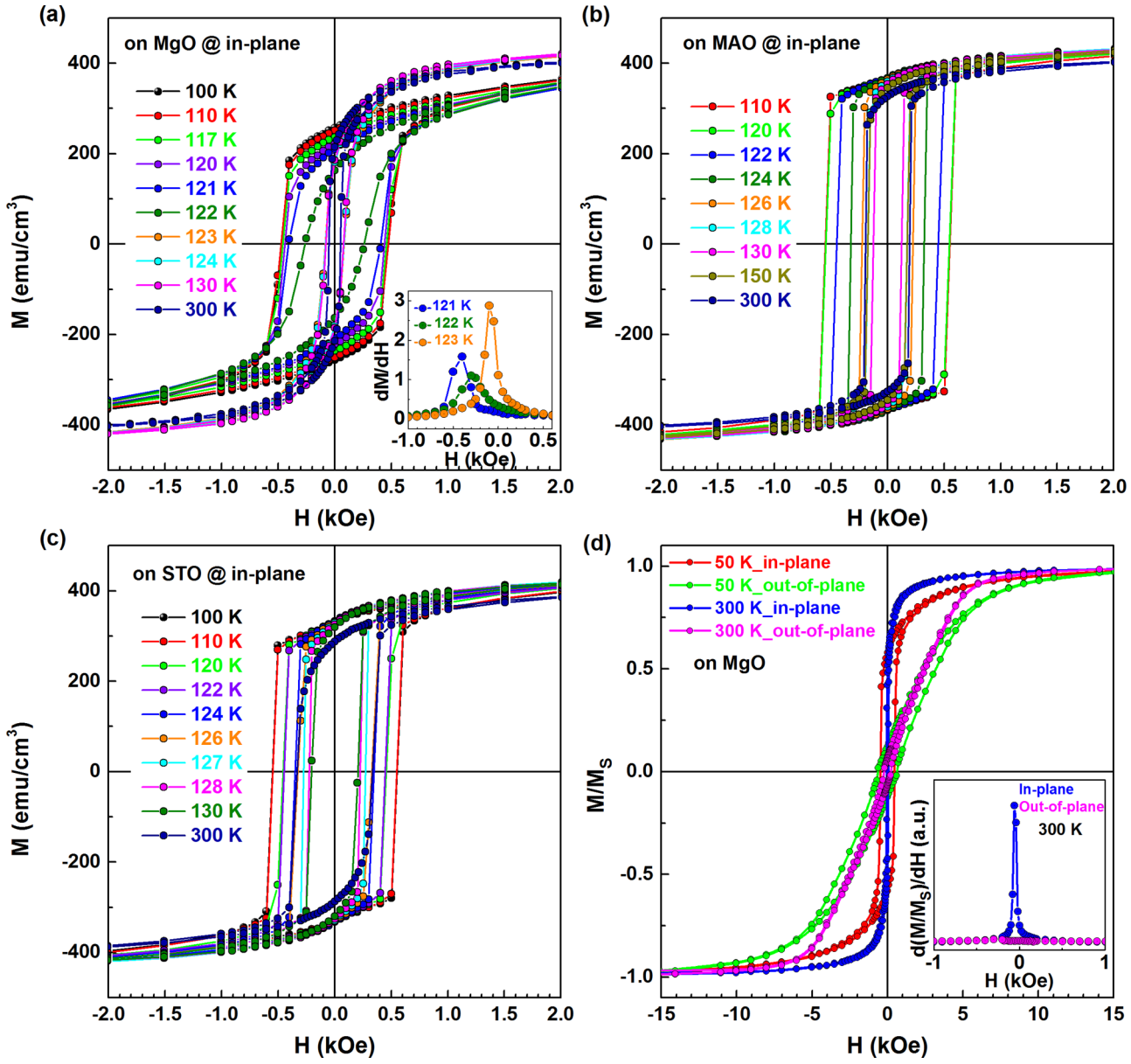

FIG. 8. In-plane magnetic hysteresis loops in applied field of 50 kOe at different temperatures for 200-nm-thick Fe_3O_4 films grown on MgO (001) (a), $MgAl_2O_4$ (001) (b), and $SrTiO_3$ (001) (c), respectively. Inset of (a): dM/dH as a function of magnetic field near the H_C at 121, 122, and 123 K. (d) Normalized magnetic hysteresis loops for in-plane and out-of-plane measured in applied field of 50 kOe at 50 and 300 K, respectively, of 200-nm-thick film grown on MgO (001). Inset: dM/dH dependent on H around the H_C at 300 K for in-plane and out-of-plane conditions.

investigation of magnetic properties of Fe_3O_4 thin films grown on different substrates. Figure 7 shows zero-field and field cooling (ZFC-FC) magnetization as a function of temperature for 200-nm-thick Fe_3O_4 thin films grown on MgO (001) (a), MAO (001) (b), and STO (001) (c), respectively, in an applied field of 200 Oe. Rapid change of magnetization at T_{V+} can be clearly seen for each ZFC curve, whereas the behavior of the FC curve is quite different for the films on MgO and on MAO or STO. An obvious reduction of magnetization at T_{V-} can be also observed for the film on MgO [Fig. 7(a)] but the variation of magnetization is very broad for the films on MAO or STO. Especially, one notices in Figs. 7(b) and 7(c) that the magnetization first increases to a maximum peak and then slowly drops with lowering temperature across T_{V-}. The dM/dT as a function of temperature near T_V [see insets of Figs. 7(a), 7(b) and 7(c)] shows two peaks at T_{V+} and T_{V-}, which are nearly consistent with those from $\rho(T)$ curves in Fig. 6, while only a clear peak at T_{V-} can be seen for the film on MgO. Therefore, the behaviors of magnetization with temperature are greatly in agreement with the transport properties of the films, in which the domain size takes a very important role.

After studying the temperature dependence of magnetization for different thin films, we then focused on the change of magnetic properties as a function of magnetic field at different temperatures. In this process, the system was first zero-field-cooled from 300 to 30 K and then the magnetic hysteresis loops $M(H)$ at different constant temperatures were

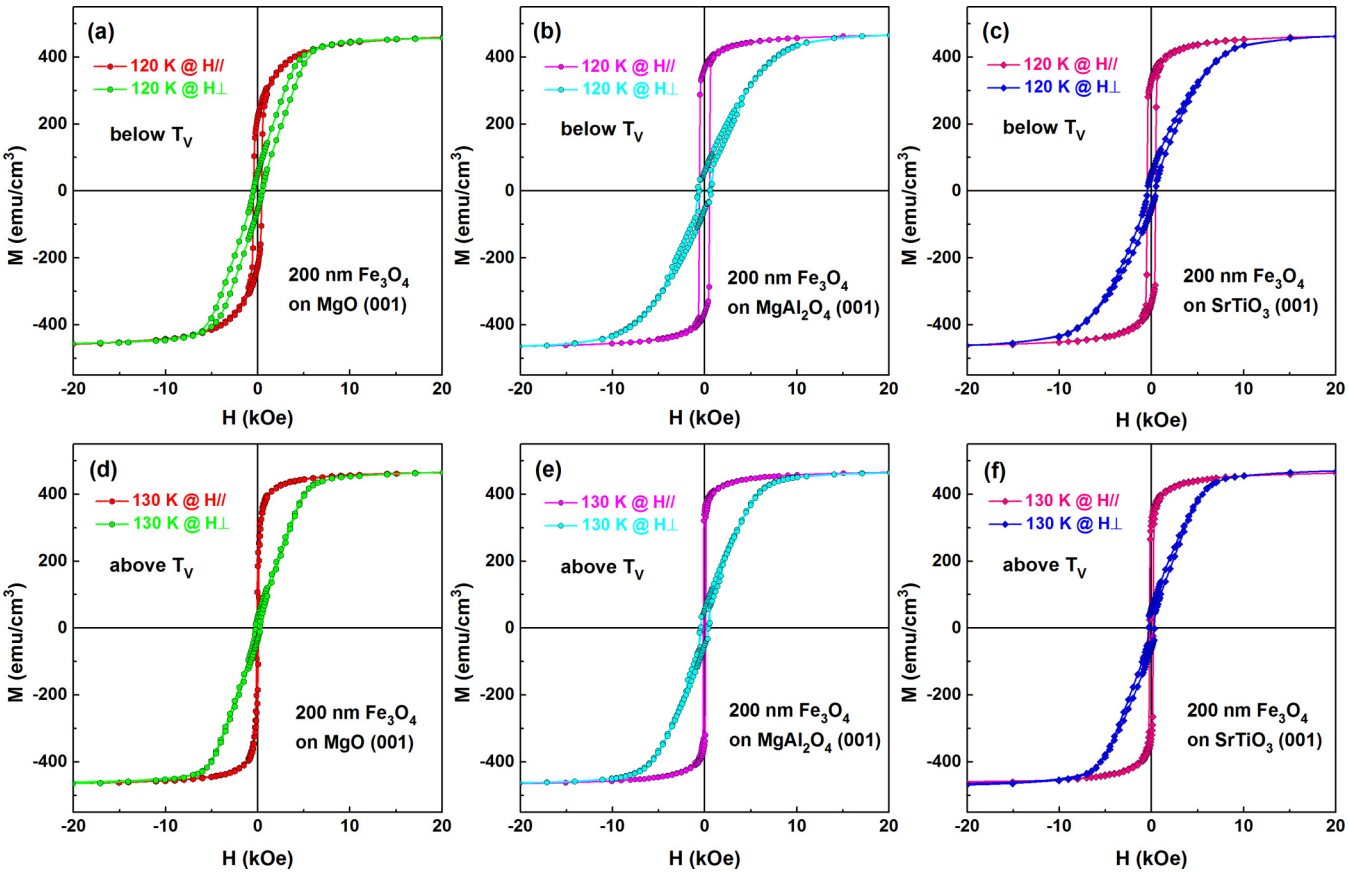

FIG. 9. In-plane ($H_{//}$) and out-of-plane ($H_{\perp}$) magnetic hysteresis loops at 120 K (below T_V) and 130 K (above T_V) for 200-nm-thick Fe_3O_4 films grown on MgO (001) (a) and (d), $MgAl_2O_4$ (001) (b) and (e), and $SrTiO_3$ (001) (c) and (f), respectively.

measured with temperature warming up from 30 to 300 K. The in-plane ($H_{//}$ along the [100] direction) $M(H)$ curves at different temperatures for 200-nm-thick Fe_3O_4 film on MgO are shown in Fig. 8(a); obviously different magnetic properties can be seen at temperatures below and above T_{V+}. At $T < 120$ K or $T > 123$ K, the variation of coercivity (H_C) or remanence (M_r) is very small; when it reaches the vicinity of T_{V+}, the H_C and the magnetization rapidly changes (see 121, 122, and 123 K). The dM/dH vs H shown as an inset of Fig. 8(a) presents a peak at H_C for each curve; the sharpest peak of about 3 emu/cm^3 Oe^{-1} with the smallest full width at half maximum (FWHM) of 130 Oe can be seen for 123 K ($>T_{V+}$), while the broadest peak of only 1 emu/cm^3 Oe^{-1} with largest FWHM of 310 Oe is found for 122 K ($= T_{V+}$). It is clear that the reversal of domains with applied magnetic field is slowest and steps across the largest field range at Verwey transition, and the relatively gradual reversal of magnetization for 121 K ($<T_{V+}$) is due to the much larger monoclinic magnetocrystalline anisotropy constant [60]. At $T > T_{V+}$, the H_C becomes quite small but the low-field magnetization is much larger than that at $T < T_{V+}$.

For comparison, the in-plane magnetic behaviors of 200-nm-thick Fe_3O_4 film grown on MAO shown in Fig. 8(b) are quite different. The $M(H)$ curves display almost rectangular shape at different temperatures including T_{V+} in which the domains are coherently reversed at H_C. Relative to the results in Fig. 8(a), with increasing temperature, we can observe a big decrease of H_C from 120 K but small change of magnetization. The low-field magnetization and the M_r slightly reduce at T_{V+}, which is much smaller than that of the film on MgO [see Fig. 8(a)]. Interestingly, H_C reaches a minimum at 130 K (120 Oe) and then gradually enhances with further increasing temperature up to 240 Oe at 300 K. At the same time, the in-plane magnetic behavior of the 200-nm-thick Fe_3O_4 film on STO shown in Fig. 8(c) is similar to that on MAO [Fig. 8(b)]. The nearly rectangular shape of the $M(H)$ curves can be observed also at different temperatures though the average domain size of this sample is only 11 nm. The H_C gradually decreases with increasing temperature and gets to a minimum value also at 130 K, and then increases to 330 Oe at 300 K. The variation trend of the low-field magnetization and the M_r around the Verwey transition is nearly the same as that in Fig. 8(b).

To further understand the magnetic properties in Fe_3O_4 thin films, we investigated the evolution of out-of-plane ($H_{\perp}$ along [001] direction) magnetic properties with temperature for Fe_3O_4 thin films grown on MgO (001), MAO (001), and STO (001). The Fe_3O_4 films grown on these three substrates have very good perpendicular anisotropic properties at different temperatures. Similarly, the out-of-plane results also show an obvious variation of some magnetic parameters at T_V. As the out-of-plane M_r is very small, the change of these values is not very sharp, especially for the films on MAO and STO, around T_V. The normalized magnetic hysteresis loops for in-plane and out-of-plane cases in an applied field of 50 kOe at 50 and 300 K, respectively, of 200-nm-thick Fe_3O_4

film on MgO is shown in Fig. 8(d). Relative to the in-plane case, the out-of-plane $M(H)$ curves show typical hard axis magnetic behaviors at 50 and 300 K respectively: large H_C, quite small M_r, and low-field magnetization, which can be clearly seen in the inset of Fig. 8(d). With respect to a sharp peak of $d(M/M_S)/dH$ at H_C for in-plane, even no peak can be found for the out-of-plane case, meaning a quite incoherent change of magnetic moments with applied magnetic field (hard axis). To better present the variation of magnetic properties around the Verwey transition, we plotted the in-plane and out-of-plane magnetic hysteresis loops at 120 K (below T_V) and 130 K (above T_V) for 200-nm-thick Fe_3O_4 films grown on MgO (001) [Figs. 9(a) and 9(d)], MAO (001) [Figs. 9(b) and 9(e)], and STO (001) [Figs. 9(c) and 9(f)], respectively. Clearly, the easy (hard) axis always stays in-plane (out-of-plane) for the three samples.

The in-plane and out-of-plane coercivity (H_C) and remanence ratio (M_r/M_S) as a function of temperature for 200-nm-thick Fe_3O_4 films grown on MgO (001), MAO (001), and STO (001) are summarized in Figs. 10(a) and 10(d), 10(b) and 10(e), and 10(c) and 10(f), respectively. We first discuss the in-plane condition; as can be seen the film on MgO has the sharpest jump of H_C at T_V, the value rapidly changes from 410 Oe at 121 K to 80 Oe at 123 K, and then it slightly reduces to only 50 Oe at 300 K, while H_C remains nearly constant at 450 Oe at $T < 120$ K. However, the change of H_C around T_V becomes very broad for the film on MAO or STO [see Figs. 10(b) and 10(c)]; it varies from 520 Oe or 450 Oe at 120 K to 120 Oe or 200 Oe at 130 K, and then increases to 190 Oe or 330 Oe at 200 K but remains nearly constant from 200 to 300 K, respectively. Moreover, one notices that the values of H_C in Figs. 10(b) and 10(c) are much larger than those in Fig. 10(a) at different temperatures, and remarkably the minimum of H_C occurs at 130 K for the former two samples. On the other hand, the out-of-plane H_C at different temperatures is larger than that of in-plane for each sample due to the hard axis. At the same time, the evolution of M_r/M_S with temperature also presents a rapid change at T_V [see Figs. 10(d), 10(e) and 10(f)]. Furthermore, the sharpest variation of M_r/M_S can be seen for the film on MgO both at in-plane and out-of-plane cases. As the good perpendicular anisotropic properties for all the films, the values of M_r/M_S for out-of-plane at different temperatures are quite small (only around 0.1). In Fig. 10(d), the in-plane M_r/M_S is around 0.58 at low temperatures, which jumps to a minimum of 0.35 at 122 K and then gradually increases to around 0.5 with further rising temperature. However, the values of in-plane M_r/M_S for the film on MAO are much larger, remaining nearly constant at about 0.78 at $T < 120$ K and reducing to about 0.7 at T_V, and then becoming nearly constant above T_V [Fig. 10(e)]. Similarly, the film on STO in Fig. 10(f) shows also very large in-plane M_r/M_S of about 0.7 below T_V and about 0.65 above T_V, respectively. In Fig. 10 it is found that the evolution of H_C and M_r/M_S in the vicinity of T_V is consistent with the electrical behaviors of the $\rho(T)$ curves in Fig. 6; the magnetic behavior for the film on MgO is quite different from that on MAO and STO.

The rapid change of H_C with temperature across T_V can be easily understood. As with the abrupt enhancement in magnetocrystalline and magnetostriction constants when Fe_3O_4 transforms from cubic ($Fd\bar{3}m$) to monoclinic (Cc) structure, the value of the dominating monoclinic magnetocrystalline anisotropy constant is about 10 times greater than the cubic anisotropy constant K_1, and thus a sharp increase of H_C is noticed at T_V [see Figs. 10(a), 10(b) and 10(c)]; the broad variation of H_C corresponds to the broad Verwey transition in Fig. 6 due to the much smaller average domain size [37]. Furthermore, we have to point out that a complete description of the evolution of the magnetic properties has to include the influence of the internal stress and the temperature dependence of the magnetostrictive and magnetoelastic energies. The different magnetic behaviors, especially the shape of $M(H)$ curves in Fig. 8, of Fe_3O_4 thin films grown on MgO and MAO have been also reported by Bollero *et al.* [44], who considered that the APBs play a very important role in the demagnetization process, that the APBs act as pinning centers for the magnetic domain walls, and that the choice of type of substrate will have a strong effect on the density of APBs [14–17,19–37].

It has been reported that the Fe_3O_4 thin films grown on MgO have a large density of APBs [14–16,24] whereas the films on MAO are expected to have a lower density of APBs due to the same structure and closer values of the lattice parameters of the film and substrate. Luysberg *et al.* [32] found that the formation mechanism of APBs in Fe_3O_4/MAO is fundamentally different from that in the Fe_3O_4/MgO system, and that the formation of misfit dislocations with partial Burgers vectors is responsible for the nucleation of APBs in Fe_3O_4/MAO. Hirth *et al.* [66–68] reported that the forces considered to be acting on the dislocations are the elastic interaction force between misfit dislocations, the homogeneous force arising from the difference in atomic volume of the constituents, and the osmotic force produced by the net vacancy flux accompanying interdiffusion. The larger the lattice mismatch between the film and the substrate, the smaller the critical thickness of the film and the higher the density of the misfit dislocations [67,68], which would generate the higher density of APBs [32]. Therefore, it can be suggested that the film on STO (mismatch −7.5%) should have more APBs than the film on MAO (−3.7%). Moreover, the XRD results in Fig. 4 give quite small average domain sizes of 11 nm and 20 nm for 200-nm-thick Fe_3O_4 films on STO and MAO, respectively, meaning much larger domain boundaries as compared to those of the film on MgO. It is clear from Figs. 8(a), 8(b) and 8(c) that the film on MgO exhibits incoherent reversal of magnetization while the films on MAO or STO show the rectangular-shaped $M(H)$ curves, which implies that the APBs and the domain size take a small role in the demagnetization process.

It is obtained from Fig. 5 that the 200-nm-thick Fe_3O_4 films grown on MgO (001) and MAO (001) show fully strained and fully relaxed states, respectively; the same thickness of film grown on a larger mismatch STO (001) should appear as fully relaxed also [64]. Quite different behaviors of the $M(H)$ curves for Fe_3O_4 thin films grown on MgO, MAO, and STO remind us to consider the very important role of strain state in the demagnetization process; the presence of strain actually retards the reversal of domains in applied magnetic field. We therefore only find incoherent change of magnetization around H_C for the film on MgO due to its fully strained state though the average domain size is much bigger than that of the films on MAO and STO. This consideration can be further confirmed

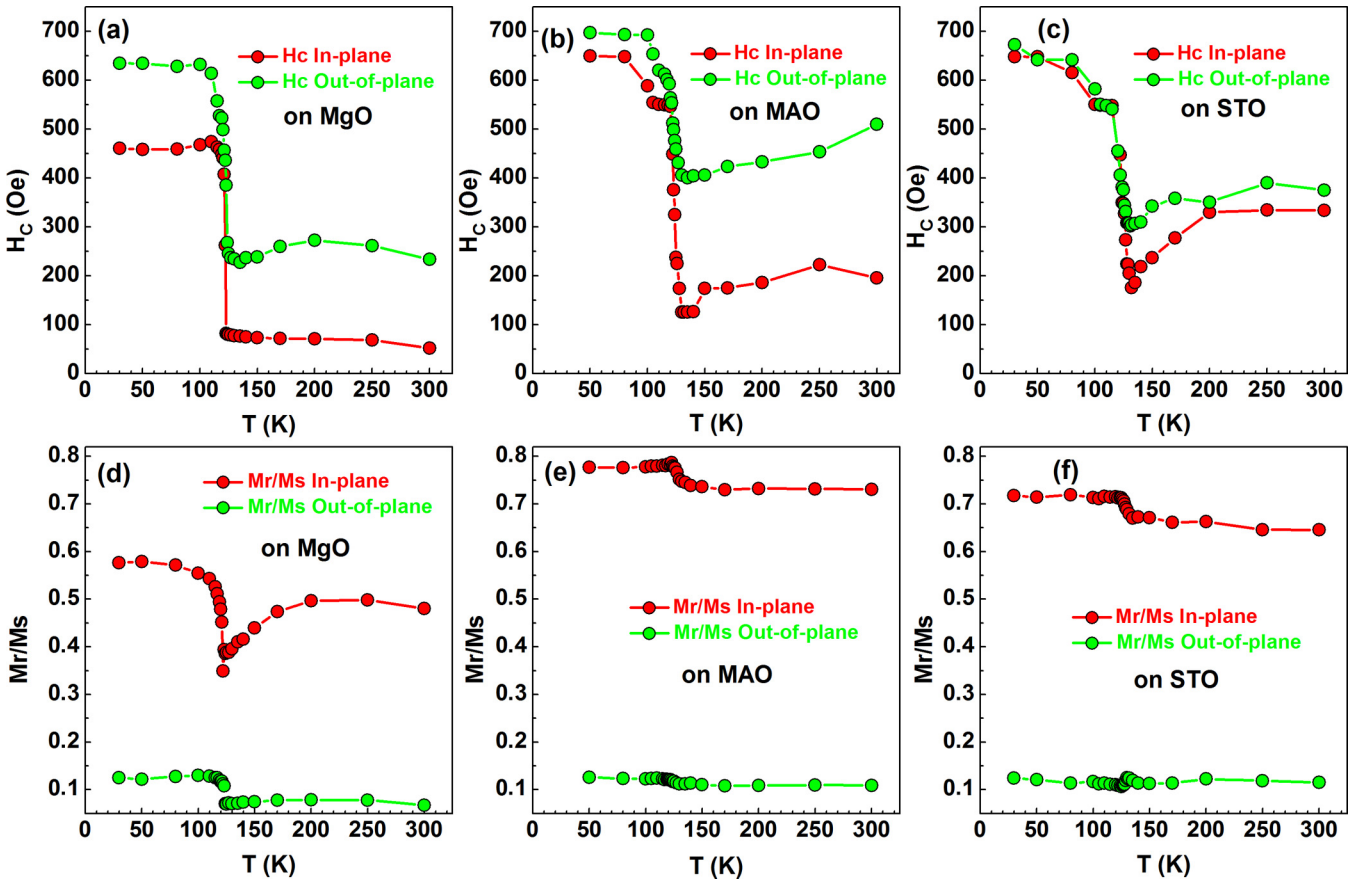

FIG. 10. Evolution of in-plane and out-of-plane H_C and M_r/M_S in dependence on the measuring temperature for 200-nm-thick Fe_3O_4 films grown on MgO (001) (a) and (d), $MgAl_2O_4$ (001) (b) and (e), and $SrTiO_3$ (001) (c) and (f), respectively.

by studying the magnetic properties in different thicknesses of Fe_3O_4 thin films grown on MAO. Figures 11(a) and 11(b) show the in-plane $M(H)$ curves of 40-nm- and 80-nm-thick Fe_3O_4 thin films grown on MAO, respectively. It is clear that the 40-nm thin film exhibits the incoherent reversal of domains like that in Fig. 8(a) while the 80-nm one presents the rectangular-shaped $M(H)$ curves similar to those in Figs. 8(b) and 8(c). From the reciprocal space mapping results, the 80-nm-thick film is nearly fully relaxed whereas the 40-nm-thick one is partial strained; therefore, it is reasonable to consider that the strain state significantly affects the demagnetization behavior of Fe_3O_4 thin films. As the thinner film has smaller domain size, we thus observe the larger H_C at temperature around and above T_V for the 40-nm thin film [see Figs. 11(c) and 11(d)], and obvious rapid change of H_C can be seen at the Verwey transition. Moreover, we note that the minimum of H_C is seen at 130 K for the films grown on MAO and STO [see Figs. 10(b) and 10(c)] but at 300 K for the film on MgO [Fig. 10(a)]. As the 200-nm-thick films grown on MAO and STO are fully relaxed, partial magnetic properties, to some extent, are closer to that of the single-crystal bulk though the domain size is much smaller. It has been reported that the absolute value of first-order cubic magnetocrystalline constant K_1 decreases rapidly with lowering temperature from 200 K and reaches zero at 130 K (isotropic point) [60], which leads to a broadening of the domain walls because the domain wall width δ_w is proportional to $K_1^{-1/2}$. As a result, the wall pinning becomes less effective resulting in a decrease of the H_C with reducing the temperature from 200 to 130 K [see Figs. 10(b) and 10(c)], similarly to the single-crystal bulk [59], which, however, is not observed in the film grown on MgO [Fig. 10(a)]. Therefore, it can be confirmed that the strain state significantly influences the magnetic properties in Fe_3O_4 thin films.

Furthermore, we found that the in-plane M_r/M_S of the film on MgO is smaller than that on MAO or STO [see Figs. 10(d), 10(e) and 10(f)]. It is theoretically calculated that the M_r/M_S is equal to 0.5 for an assembly of uniaxial particles oriented at random [69], and of 0.831 and 0.866 for positive and negative K_1, respectively, of the cubic magnetocrystalline anisotropy materials [70,71]. Dionne reported the relationship between the remanence ratio and the stress, the magnetostriction constants (λ_{100} and λ_{111}), and K_1 of the cubic crystal structure; M_r/M_S reduces with increasing tensile stress when $K_1 < 0$ and $\lambda_{100} < 0$ [72,73]. For Fe_3O_4 thin films, the K_1 and λ_{100} are negative above T_V [15,60]; thus the smaller in-plane M_r/M_S of the film on MgO is observed. Similar phenomena are also found in $CoFe_2O_4$ or $NiFe_2O_4$ thin films grown on a piezoelectric substrate [74,75]. Moreover, another property of the in-plane M_r/M_S vs T curve for three samples is also seen in Figs. 10(d), 10(e) and 10(f): a greater M_r/M_S for temperatures below T_V than above T_V. It is reported that the easy (hard) axis changes from the [111] ([100]) to [100] ([111]) direction with lowering temperature from high temperature to

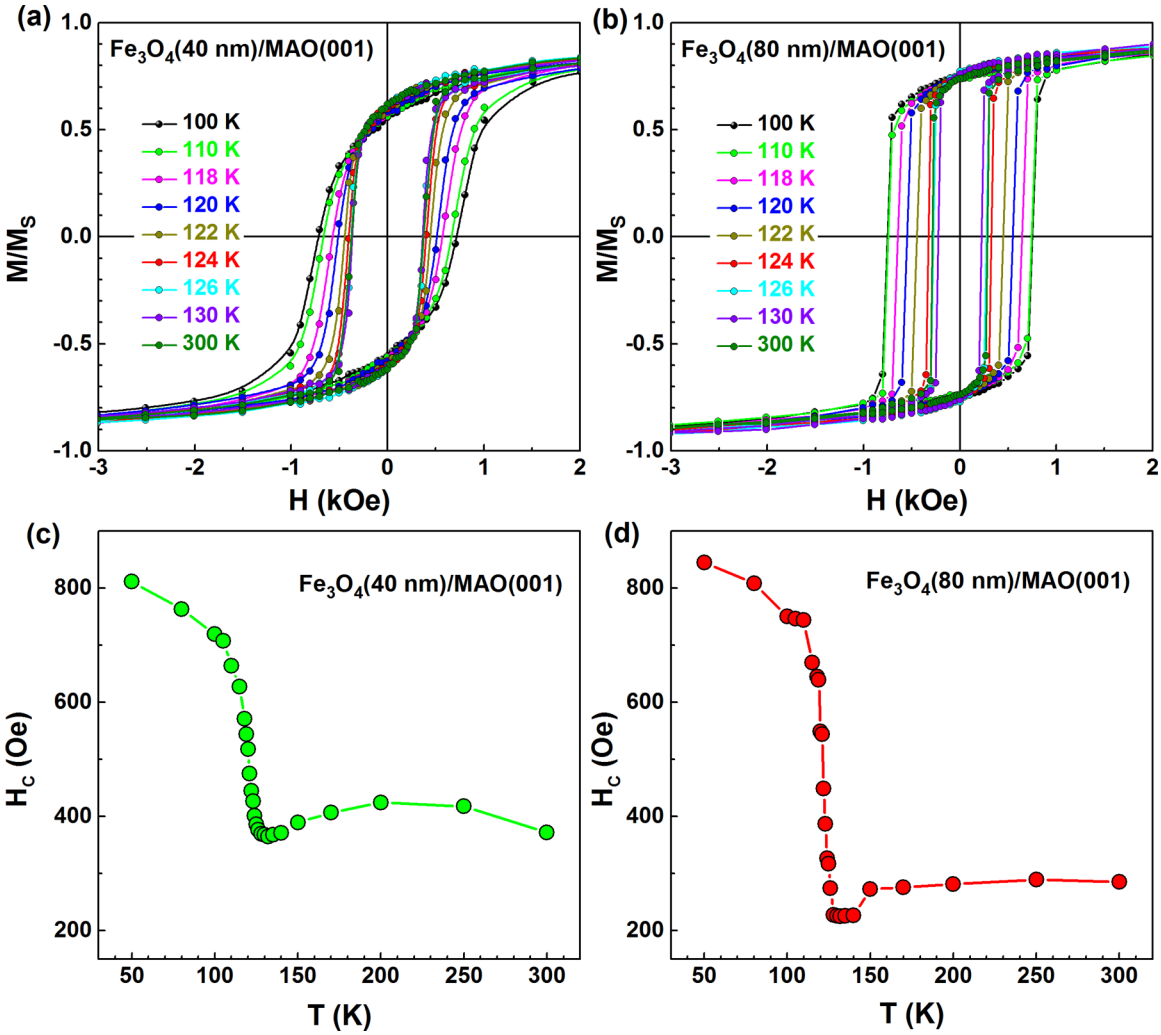

FIG. 11. In-plane magnetic hysteresis loops in applied field of 50 kOe at different temperatures for (a) 40-nm- and (b) 80-nm-thick Fe_3O_4 thin films grown on $MgAl_2O_4$ (001). Temperature dependence of in-plane H_C for (c) 40-nm- and (d) 80-nm-thick Fe_3O_4 thin films grown on $MgAl_2O_4$ (001).

below T_V for bulk magnetite [53,54,60], whereas the easy axis always remains in the [100] direction in our thin films at all temperature ranges. It could be considered that the easy magnetization direction may slightly deviate from [100] for very thick film (200 nm) at $T > T_V$, which would influence the remanence ratio; thus the higher M_r/M_S at temperatures below T_V can be observed for very thick film.

To more comprehensively understand the magnetic behaviors in Fe_3O_4 thin films, we also investigated the magnetic properties of 40-nm- and 80-nm-thick films on MgO (001); the films on MgO are all fully strained (we thus do not need to consider the influence of strain state) and the H_C and M_r/M_S for three thicknesses as a function of temperature are plotted in Figs. 12(a) and 12(b), respectively. As can be seen all the samples exhibit very sharp jump of H_C at their Verwey transitions, respectively. The value of H_C obviously reduces with increasing thickness below or above T_V due to the great increase of average domain size from 33 nm for 40-nm- to 98 nm for 200-nm-thick Fe_3O_4 film, while the demagnetization behaviors are nearly the same for three samples because of the same strain state. It is observed that the change of M_r/M_S at T_V is different for three samples. An obvious increase and decrease of M_r/M_S is seen for 40-nm- and 200-nm-thick films, respectively, whereas the 80-nm-thick one has a special behavior, which presents the decrease of M_r/M_S below T_V, like that of the 200-nm film, but a sharp increase of M_r/M_S at T_V, similar to that of the 40-nm one, and then remains nearly constant above T_V. The absolute difference of M_r/M_S below and above T_V is much smaller than that of 40-nm- or 200-nm-thick films. Therefore, it is very interesting that we actually find a clear reversal of M_r/M_S from increase to decrease jump at T_V with increasing thickness, and the critical thickness is about 80 nm. At high temperature, the easy axis is towards the [111] direction for bulk magnetite [53,54,60] but stays in the [100] direction in our thin films. For the thinner Fe_3O_4 films, the interface effect is stronger; the easy axis of the domains can be more uniformly oriented to [100], and thus the larger M_r/M_S for the thinner films above T_V can be seen. On the other hand, the interface effect would play a more important role for the smaller anisotropy constant condition, which might lead to the increase in M_r/M_S with rising temperature from below to above T_V for very thin film.

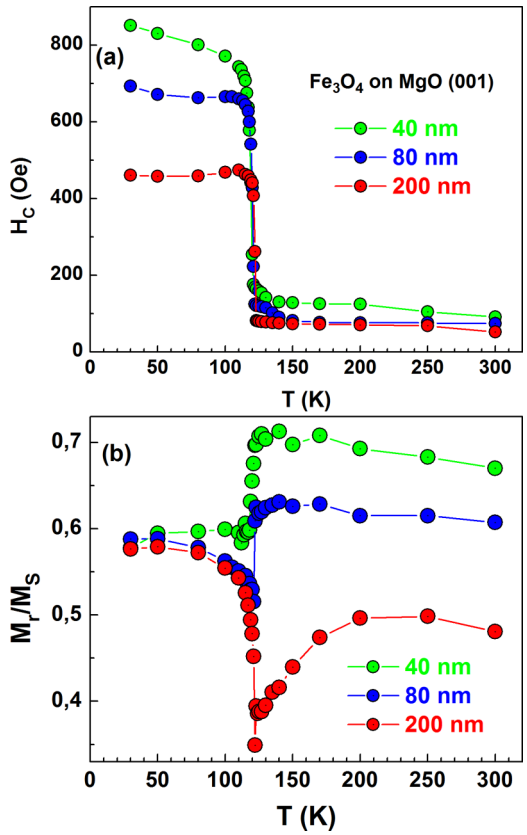

FIG. 12. In-plane H_C (a) and M_r/M_S (b) as a function of temperature for 40-nm-, 80-nm-, and 200-nm-thick Fe_3O_4 thin films grown on MgO (001).

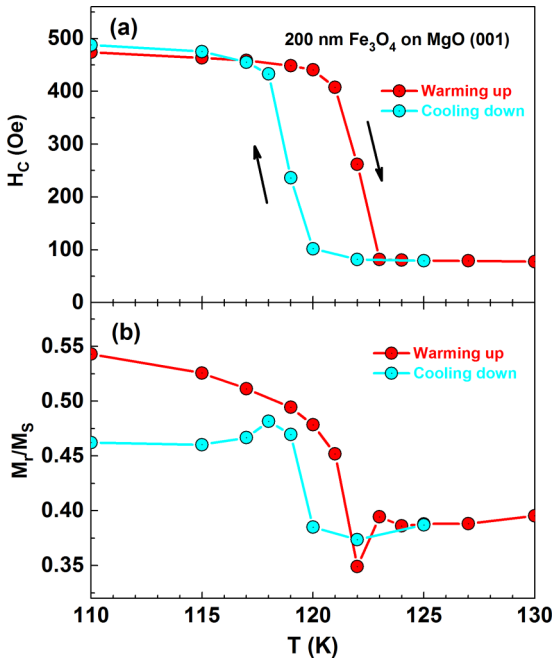

FIG. 13. H_C (a) and M_r/M_S (b) as a function of temperature for cooling down and warming up branches in the vicinity of T_V of 200-nm-thick Fe_3O_4 film grown on MgO (001).

Finally, we note that the $\rho(T)$ curve of Fe_3O_4 thin film grown on MgO at the Verwey transition shows a big hysteresis (~4 K) (see Fig. 6); it is expected that the magnetic properties should rapidly change at T_{V-} and T_{V+}, and thus a big hysteretic loop can be seen. To observe this phenomenon, we measured $M(H)$ curves with temperature along the cooling down and warming up branches near the T_V. The H_C and M_r/M_S as a function of temperature in the vicinity of T_V are plotted in Figs. 13(a) and 13(b), respectively. A big hysteretic loop (~4 K) of the $H_C(T)$ curve with a sharp jump of H_C at T_{V-} and T_{V+}, respectively, is clearly observed [Fig. 13(a)]. At temperatures deviating from T_V, the H_C is nearly the same for the two different measurement processes. The M_r/M_S vs T in Fig. 13(b) also shows a rapid change at T_{V-} and T_{V+}, respectively, despite that the hysteretic loop is not so obvious as the H_C. For the Fe_3O_4 thin films grown on MAO or STO, the hysteretic loop is very narrow (~1 K) and the transition is very broad (Fig. 6); accordingly, the variation of magnetic properties becomes very slow, and it is not easy to distinguish the change of magnetic properties at T_{V-} and T_{V+}, respectively.

VI. CONCLUSION

To summarize, we have systematically investigated the evolution of magnetic properties with temperature in high-quality epitaxial Fe_3O_4 thin films grown on MgO (001), MAO (001), and STO (001) substrates. We observed rapid variations of magnetization, H_C, and M_r/M_S at T_V, which are consistent with the behaviors of $\rho(T)$ curves for the thin films on different substrates. In particular, we found quite different magnetic behaviors with temperature for the thin films on MgO from those on MAO and STO, in which the domain size and the strain state play very important roles. The H_C is mainly determined by the domain size but the demagnetization process is mainly dependent on the strain state. The small domain size and high strain state result in large coercivity and incoherent reversal of magnetization, respectively. The minimum of H_C at 130 K can be seen for the films on MAO and STO, similar to that of the single-crystal bulk, due to the fully relaxed state, but the smallest H_C is found at 300 K for the films on MgO. Furthermore, we found a smaller remanence ratio for the film grown on MgO than that on MAO and STO, which is induced from the tensile strain effect. Moreover, we observed a very interesting reversal of remanence ratio at T_V with thickness for the Fe_3O_4 thin films grown on MgO: from a rapid enhancement for 40-nm- to a sharp drop for 200-nm-thick film, and the critical thickness is about 80 nm; the interface effect should play a very important role in this phenomenon. Finally, a clear hysteretic loop of H_C (or M_r/M_S) with temperature around T_V, corresponding to the loop of the $\rho(T)$ curve, was seen in Fe_3O_4 thin film grown on MgO. Our work will give a more comprehensive understanding of magnetic behaviors in Fe_3O_4 thin films.

ACKNOWLEDGMENTS

The authors would like to thank Prof. Liu Hao Tjeng and Dr. Chun-Fu Chang for useful discussion. The research of X.H.L. was supported by the Max Planck POSTECH Center for Complex Phase Materials. W.L. and Z.D.Z. were supported

by the National Natural Science Foundation of China under Projects No. 51590883 and No. 51331006, and as a project of the Chinese Academy of Sciences with Grant No. KJZD-EW-M05-3.

[1] F. Walz, J. Phys.: Condens. Matter **14**, R285 (2002).
[2] J. García and G. Subías, J. Phys.: Condens. Matter **16**, R145 (2004).
[3] R. A. de Groot, F. M. Mueller, P. G. van Engen, and K. H. J. Buschow, Phys. Rev. Lett. **50**, 2024 (1983).
[4] A. Yanase and K. Siratori, J. Phys. Soc. Jpn. **53**, 312 (1984).
[5] R. A. de Groot, F. M. Mueller, P. G. van Engen, and K. H. J. Buschow, J. Appl. Phys. **55**, 2151 (1984).
[6] R. A. de Groot and K. H. J. Buschow, J. Magn. Magn. Mater. **54–57**, 1377 (1986).
[7] E. J. W. Verwey, Nature (London) **144**, 327 (1939).
[8] X. W. Li, A. Gupta, G. Xiao, W. Qian, and V. P. Dravid, Appl. Phys. Lett. **73**, 3282 (1998).
[9] P. Seneor, A. Fert, J. L. Maurice, F. Montaigne, F. Petroff, and A. Vaurès, Appl. Phys. Lett. **74**, 4017 (1999).
[10] G. Hu and Y. Suzuki, Phys. Rev. Lett. **89**, 276601 (2002).
[11] F. Greullet, E. Snoeck, C. Tiusan, M. Hehn, D. Lacour, O. Lenoble, C. Magen, and L. Calmels, Appl. Phys. Lett. **92**, 053508 (2008).
[12] G. M. Müller, J. Walowski, M. Djordjevic, G. X. Miao, A. Gupta, A. V. Ramos, K. Gehrke, V. Moshnyaga, K. Samwer, J. Schmalhorst, A. Thomas, A. Hütten, G. Reiss, J. S. Moodera, and M. Münzenberg, Nat. Mater. **8**, 56 (2009).
[13] Z. M. Liao, H. C. Wu, J. J. Wang, G. L. W. Cross, S. Kumar, I. V. Shvets, and G. S. Duesberg, Appl. Phys. Lett. **98**, 052511 (2011).
[14] J. B. Moussy, J. Phys. D: Appl. Phys. **46**, 143001 (2013).
[15] D. T. Margulies, F. T. Parker, F. E. Spada, R. S. Goldman, J. Li, R. Sinclair, and A. E. Berkowitz, Phys. Rev. B **53**, 9175 (1996).
[16] D. T. Margulies, F. T. Parker, M. L. Rudee, F. E. Spada, J. N. Chapman, P. R. Aitchison, and A. E. Berkowitz, Phys. Rev. Lett. **79**, 5162 (1997).
[17] J. B. Moussy, S. Gota, A. Bataille, M. J. Guittet, M. Gautier-Soyer, F. Delille, B. Dieny, F. Ott, T. D. Doan, P. Warin, P. Bayle-Guillemaud, C. Gatel, and E. Snoeck, Phys. Rev. B **70**, 174448 (2004).
[18] G. Q. Gong, A. Gupta, G. Xiao, W. Qian, and V. P. Dravid, Phys. Rev. B **56**, 5096 (1997).
[19] S. B. Ogale, K. Ghosh, R. P. Sharma, R. L. Greene, R. Ramesh, and T. Venkatesan, Phys. Rev. B **57**, 7823 (1998).
[20] X. W. Li, A. Gupta, G. Xiao, and G. Q. Gong, J. Appl. Phys. **83**, 7049 (1998).
[21] M. Ziese and H. J. Blythe, J. Phys.: Condens. Matter **12**, 13 (2000).
[22] M. Ziese, R. Hohne, H. C. Semmelhack, H. Reckentin, N. H. Hong, and P. Esquinazi, Eur. Phys. J. B **28**, 415 (2002).
[23] M. Ziese, Rep. Prog. Phys. **65**, 143 (2002).
[24] W. Eerenstein, T. T. M. Palstra, T. Hibma, and S. Celotto, Phys. Rev. B **66**, 201101(R) (2002).
[25] W. Eerenstein, T. T. M. Palstra, S. S. Saxena, and T. Hibma, Phys. Rev. Lett. **88**, 247204 (2002).
[26] S. K. Arora, R. G. S. Sofin, and I. V. Shvets, Phys. Rev. B **72**, 134404 (2005).
[27] A. V. Ramos, J. B. Moussy, M. J. Guittet, A. M. Bataille, M. Gautier-Soyer, M. Viret, C. Gatel, P. Bayle-Guillemaud, and E. Snoeck, J. Appl. Phys. **100**, 103902 (2006).
[28] S. K. Arora, R. G. S. Sofin, I. V. Shvets, and M. Luysberg, J. Appl. Phys. **100**, 073908 (2006).
[29] R. Kumar, M. Wasi Khan, J. P. Srivastava, S. K. Arora, R. G. S. Sofin, R. J. Choudhary, and I. V. Shvets, J. Appl. Phys. **100**, 033703 (2006).
[30] R. Ramos, S. K. Arora, and I. V. Shvets, Phys. Rev. B **78**, 214402 (2008).
[31] D. S. Lee and G. Chern, Solid State Commun. **148**, 353 (2008).
[32] M. Luysberg, R. G. S. Sofin, S. K. Arora, and I. V. Shvets, Phys. Rev. B **80**, 024111 (2009).
[33] R. G. S. Sofin, S. K. Arora, and I. V. Shvets, Phys. Rev. B **83**, 134436 (2011).
[34] A. Hamie, Y. Dumont, E. Popova, A. Fouchet, B. Warot-Fonrose, C. Gatel, E. Chikoidze, J. Scola, B. Berini, and N. Keller, Thin Solid Films **525**, 115 (2012).
[35] A. Kumar, D. K. Pandya, and S. Chaudhary, J. Appl. Phys. **111**, 073901 (2012).
[36] D. Gilks, L. Lari, J. Naughton, O. Cespedes, Z. Cai, A. Gerber, S. M. Thompson, K. Ziemer, and V. K. Lazarov, J. Phys.: Condens. Matter **25**, 485004 (2013).
[37] X. H. Liu, A. D. Rata, C. F. Chang, A. C. Komarek, and L. H. Tjeng, Phys. Rev. B **90**, 125142 (2014).
[38] I. Bernal-Villamil and S. Gallego, J. Phys.: Condense. Matter **27**, 293202 (2015).
[39] P. A. A. van der Heijden, P. J. H. Bloemen, J. M. Gaines, J. T. W. M. van Eemeren, R. M. Wolf, P. J. van der Zaag, and W. J. M. de Jonge, J. Magn. Magn. Mater. **159**, L293 (1996).
[40] P. A. A. van der Heijden, M. G. van Opstal, C. H. W. Swuste, P. H. J. Bloemen, J. M. Gaines, and W. J. M. de Jonge, J. Magn. Magn. Mater. **182**, 71 (1998).
[41] F. C. Voogt, T. T. M. Palstra, L. Niesen, O. C. Rogojanu, M. A. James, and T. Hibma, Phys. Rev. B **57**, R8107(R) (1998).
[42] W. Eerenstein, T. Hibma, and S. Celotto, Phys. Rev. B **70**, 184404 (2004).
[43] Y. Zhou, X. Jin, and I. V. Shvets, J. Appl. Phys. **95**, 7357 (2004).
[44] A. Bollero, M. Ziese, R. Hohne, H. C. Semmelhack, U. Kohler. A. Setzer, and P. Esquinazi, J. Magn. Magn. Mater. **285**, 279 (2005).
[45] F. Delille, B. Dieny, J. B. Moussy, M. J. Guittet, S. Gota, M. Gautier-Soyer, and C. Marin, J. Magn. Magn. Mater. **294**, 27 (2005).
[46] S. K. Arora, H. C. Wu, R. J. Choudhary, I. V. Shvets, O. N. Mryasov, H. Yao, and W. Y. Ching, Phys. Rev. B **77**, 134443 (2008).
[47] J. Orna, P. A. Algarabel, L. Morellon, J. A. Pardo, J. M. de Teresa, R. Lopez Anton, F. Bartolome, L. M. Garcia, J. Bartolome, J. C. Cezar, and A. Wildes, Phys. Rev. B **81**, 144420 (2010).
[48] P. Prieto, J. E. Prieto, R. Gargallo-Caballero, J. F. Marco, and J. de la Figuera, Appl. Surf. Science **359**, 742 (2015).
[49] B. L. Chen, Z. Ding, D. H. Ma, J. X. Li, X. Xiao, and Y. Z. Wu, Phys. Lett. A **379**, 1780 (2015).

[50] S. Alraddadi, W. Hines, T. Yilmaz, G. D. Gu, and B. Sinkovic, J. Phys.: Condens. Matter **28**, 115402 (2016).
[51] X. H. Liu, C. F. Chang, A. D. Rata, A. C. Komarek, and L. H. Tjeng, npj Quantum Materials **1**, 16027 (2016).
[52] C. A. Domenicali, Phys. Rev. **78**, 458 (1950).
[53] B. A. Calhoun, Phys. Rev. **94**, 1577 (1955).
[54] S. Umemura and S. Iida, J. Phys. Soc. Jpn. **40**, 679 (1976).
[55] K. Abe, Y. Miyamoto, and S. Chikazumi, J. Phys. Soc. Jpn. **41**, 1894 (1976).
[56] Z. Kakol and J. M. Honig, Phys. Rev. B **40**, 9090 (1989).
[57] R. Aragon, Phys. Rev. B **46**, 5328 (1992).
[58] O. Ozdemir and D. J. Dunlop, Earth Planet. Sci. Lett. **165**, 229 (1999).
[59] A. R. Muxworthy, Earth Planet. Sci. Lett. **169**, 51 (1999).
[60] A. R. Muxworthy and E. McClelland, Geophys. J. Int. **140**, 101 (2000).
[61] S. A. Chambers and S. A. Joyce, Surf. Sci. **420**, 111 (1999).
[62] S. A. Chambers, R. F. C. Farrow, S. Maat, M. F. Toney, L. Folks, J. G. Catalano, T. P. Trainor, and G. E. Brown, Jr., J. Magn. Magn. Mater. **246**, 124 (2002).
[63] DS $= 0.9\lambda_{\mathrm{Cu}}/(B_{\mathrm{struct}}\cos\theta)$, where λ_{Cu} is 1.54056 Å, B_{struct} describes the structural broadening, which is the difference in integral profile width between a standard (0.006) and the sample to be analyzed, and θ is the angle of incidence.
[64] A. Fischer, H. Kuhne, and H. Richter, Phys. Rev. Lett. **73**, 2712 (1994).
[65] F. E. N. Ramirez and J. A. Souza, Braz. J. Phys. **44**, 308 (2014).
[66] K. Shinohara and J. P. Hirth, Philos. Mag. **27**, 883 (1973).
[67] J. P. Hirth and X. Feng, J. Appl. Phys. **67**, 3343 (1990).
[68] J. P. Hirth, Acta. Mater. **48**, 93 (2000).
[69] E. C. Stoner and E. P. Wohlfarth, Philos. Trans. R. Soc. London, Ser. A **240**, 599 (1948).
[70] J. García-Otero, M. Porto, J. Rivas, and A. Bunde, J. Appl. Phys. **85**, 2287 (1999).
[71] J. Geshev, L. G. Pereira, J. E. Schmidt, and M. Mikhov, J. Appl. Phys. **90**, 6243 (2001).
[72] G. F. Dionne, IEEE Trans. Magn. **5**, 596 (1969).
[73] G. F. Dionne, IEEE Trans. Magn. **7**, 715 (1971).
[74] J. H. Park, J. H. Lee, M. G. Kim, Y. K. Jeong, M. A. Oak, H. M. Jang, H. J. Choi, and J. F. Scott, Phys. Rev. B **81**, 134401 (2010).
[75] J. H. Park, Y. K. Jeong, S. Ryu, J. Y. Son, and H. M. Jang, Appl. Phys. Lett. **96**, 192504 (2010).